Robust fibre-optic sensor arrays for monitoring early-age performance of mass-produced concrete sleepers

Butler, Liam J.; Xu, Jinlong; He, Ping; Gibbons, Niamh; Dirar, Samir; Middleton, Campbell; Elshafie, Mohammed

DOI:
10.1177/1475921717714615

Robust Fibre-Optic Sensor Arrays for Monitoring Early-Age Performance of Mass-Produced Concrete Sleepers

Liam J. Butler[*1], Jinlong Xu[2], Ping He[3], Niamh Gibbons[1], Samir Dirar[4], Campbell Middleton[1], and Mohammed Elshafie[1]
[1] Department of Engineering, University of Cambridge, UK
[2] School of Civil Engineering, Harbin Institute of Technology, China
[3] Department of Geotechnical Engineering, Tongji University, China
[4] Department of Civil Engineering, University of Birmingham, UK
[*] Corresponding author email: LB643@cam.ac.uk

Abstract

This study investigates integrating fibre optic sensing technology into the production process of concrete railway sleepers. Robust fibre Bragg grating (FBG) strain and temperature sensor arrays were developed specifically for this application and were designed for long-term monitoring of sleeper performance. The sensors were used to monitor sleeper production and to help gain a deeper understanding of their early-age behaviour which can highly influence long-term performance. Twelve sleepers were instrumented and strain data were collected during the entire manufacturing process including concrete casting and curing, prestressing strand detensioning, and qualification testing. Following the production process, sleepers were stored temporarily and monitored for four months until being placed in service. The monitoring results highlight the intrinsic variability in strain development among identical sleepers, despite high levels of production quality control. Using prestress loss as a quality control indicator, the integrated sensing system demonstrated that sleepers were performing within Eurocode-based design limits prior to being placed in service. A 3D nonlinear finite element (FE) model was developed to provide additional insight into the sleepers' early-age behaviour. Based on the FBG-calibrated FE model, more realistic estimates for the creep coefficient were provided and found to be 48% of the Eurocode-predicted values.

1.0 Introduction

Railways play a significant role in the social and economic growth of many countries around the world providing a safe and convenient option for transporting freight and passengers. The UK rail network alone is a £13.5 billion industry with a total of 1.69 billion passenger journeys recorded in 2014-15 which has increased by 130% compared to 1994/95 values [1] and is expected to rise by another 400 million passenger journeys by 2020 [2]. As a result, the rail network represents a critical piece of infrastructure in the UK that requires constant maintenance, planning and innovation to ensure that its future performance is adequately safeguarded. A critical component of the rail network is the track bed system itself which comprises the subgrade, ballast, sleepers, fasteners, and rails. In particular, the sleepers are the primary structural components which carry the wheel loads from the rolling stock, to the rails, and into the ballast. Sleepers are primarily designed for dynamic loads and the way in which the dynamic loads are distributed into the supporting ballast is highly dependent on the condition of the ballast itself. Furthermore, the sleeper materials and their manufacturing process can have considerable influence on both their short and long term performance [3]. Therefore, monitoring sleepers throughout their entire life would provide invaluable information to rail asset managers on the performance of this critical component of the rail network.

Prestressed concrete sleeper design and research have been evolving over the past several decades since the first prestressed concrete sleepers were first introduced in the UK in the 1940's [4]. There have, however, been very few studies that have investigated integrating a sufficiently durable sensing system directly into the sleeper manufacturing process with the aim of understanding variations during production, early-age performance and their influence on long-term performance. In 2012, Carlsson carried out a comprehensive laboratory study directed at determining the influence that production process has on early performance of

prestressed concrete sleepers [3]. Numerical models simulating the thermal and structural response were developed and compared with measurements of sleepers produced at several pre-casting facilities. The study identified various parameters during the production process that, if properly controlled, could help to reduce the amount of early-age prestress losses. Another study by Loaec et al (2014) described embedding FBG (fibre Bragg grating) fibre optic sensors into concrete sleepers [5]. This study primarily involved static and dynamic laboratory testing. They purported that their study tried to address the lack of consensus by rail experts in determining the effective bending moments in the sleepers over their long term in-service behaviour. Experimental results showed that the system was capable of providing linear and repeatable results; however, no case studies evolving from this work have been reported. Sadeghi (2010) installed load cells within the tops and bottoms of several sleepers during their manufacture [6]. Using the load cells together with several accelerometers, they investigated both the load distribution and the dynamic response of the sleepers under real conditions and loadings. A variety of other studies have been carried out which consider the structural response of prestressed concrete sleepers; however, they have involved mainly external monitoring devices under controlled laboratory conditions [7, 8, 9, 10]. There have also been a limited number of numerical studies that have employed finite element analysis to help better understand sleeper performance. Kaewunruen and Remennikov (2006) developed a 3D non-linear finite element model of a prestressed concrete sleeper and simulated the sleeper response due to the transfer of the prestressing force and compared their model predictions with bending test results to determine appropriate concrete material models [11]. González-Nicieza et al. (2008) developed a 3D elastic model to analyse the failure of concrete sleepers in heavy haul railway tracks. The numerical results were employed to integrate the limited information from laboratory and in-situ field testing in order to identify more precisely the causes of track failure [12].

Fibre optic based sensors are finding increasing applications for use in monitoring a wide variety of the civil engineering infrastructure. Compared to conventional electrical-based sensors, fibre optic sensors are chemically inert (not subject to corrosion), non-conductive, and can be multiplexed along a single cable (avoiding multiple bundles of copper wire cabling). McKeeman et al. (2016) used metal-encapsulated FBGs to measure prestress levels in laboratory-produced beams with aims of using the system in various containment structures exposed to harsh industrial environments [13]. Likewise, railway sleepers are also subjected to severely harsh conditions during their lifetime, leading to ageing and deterioration problems. Therefore, a sensing system must be sufficiently robust in order to survive during a sleepers' design life (typically between 30 and 50 years). By integrating a robust array of fibre optic sensors directly into the sleeper manufacturing process, the entire strain history of a sleeper may be recorded and monitored during its service life. The UK rail operator, Network Rail, predicts that more than 900 km of track in the UK rail network require sleeper replacement; and approximately 70% of the sleepers are concrete sleepers [14]. Implementing a representative number of self-sensing sleepers at key locations within the rail network would allow stakeholders to gain better long-term insights into how these sleepers behave in-service and could help inform intervention and/or replacement decisions.

This paper describes the development of a robust fibre optic sensing array and its integration into the highly-controlled railway sleeper manufacturing process. It demonstrates how integrated sensing can help to better understand both the production process (and its effect on quality) and early-age behaviour of prestressed concrete sleepers which can significantly affect their long-term performance. This work complements an earlier pilot study [15] and forms part of a future project which will involve full-scale laboratory tests and in-situ monitoring of concrete sleepers under live train loading.

2.0 Experimental Monitoring Programme

2.1 Sleeper manufacturing process

The sleepers monitored as part of this study were manufactured at CEMEX's sleeper production facility in Birmingham, UK. The sleeper manufacturing process consisted of multiple stages. First, the sleeper moulds (casting beds) were cleaned and the end plates fastened. Next, the prestressing strands were run along the entire length of the prestressing beds and placed in the sleeper moulds. Strands were then stressed up to 75% of their yield capacity (approximately 1327 MPa). After the cables were stressed, concrete pouring commenced at the end of the bay where the tendons were jacked and finished at the other end where the tendons were anchored. Concrete was batched in the facility and was placed using an automated hopper system. Concrete quality was monitored during the entire casting process to control the consistency between successive batches. Once concrete casting was completed, the beds were covered by plastic sheets and dampened burlap to prevent excess moisture from evaporating from the concrete surface. The casting beds were temperature controlled and thermocouples were installed within the fresh concrete at several locations along the casting bay to monitor curing temperatures. The temperature measurements were used to correlate concrete maturity and compressive strength. After approximately 18 hours of curing, the concrete achieved the required minimum compressive strength (35 MPa) for transferring the prestress force (detensioning). Prior to releasing the prestressing strands, a small additional tension force was introduced in order to loosen the hydraulic jack clamps. The prestressing beds at the CEMEX factory have been specially designed on rollers, which allow for a 'soft' detensioning of the strands to avoid cracking within the early age concrete due to the sudden load change. Once all of the prestressing force had been released, the strands between each mould were cut using an automated band saw. The mould end plates were then removed and an overhead crane lifted the sleepers off the bed and onto pallets for storage and transport.

2.2 Robust fibre optic sensor array development

Fibre optic sensors based on fibre Bragg gratings (FBGs) were used in this study. The FBG sensor arrays were developed at the University of Cambridge specifically for installation in prestressed concrete sleepers. FBGs used during this study were manufactured using draw tower technology by which the gratings were inscribed during the glass fibre drawing process which maintains the original fibre strength. Figure 1 illustrates the sensor arrangement for a typical type G44 sleeper. A four channel FBG analyser (Micron Optics sm310) was used to interrogate the sensors which is capable of sampling up to 1000 Hz with a ±5με resolution.

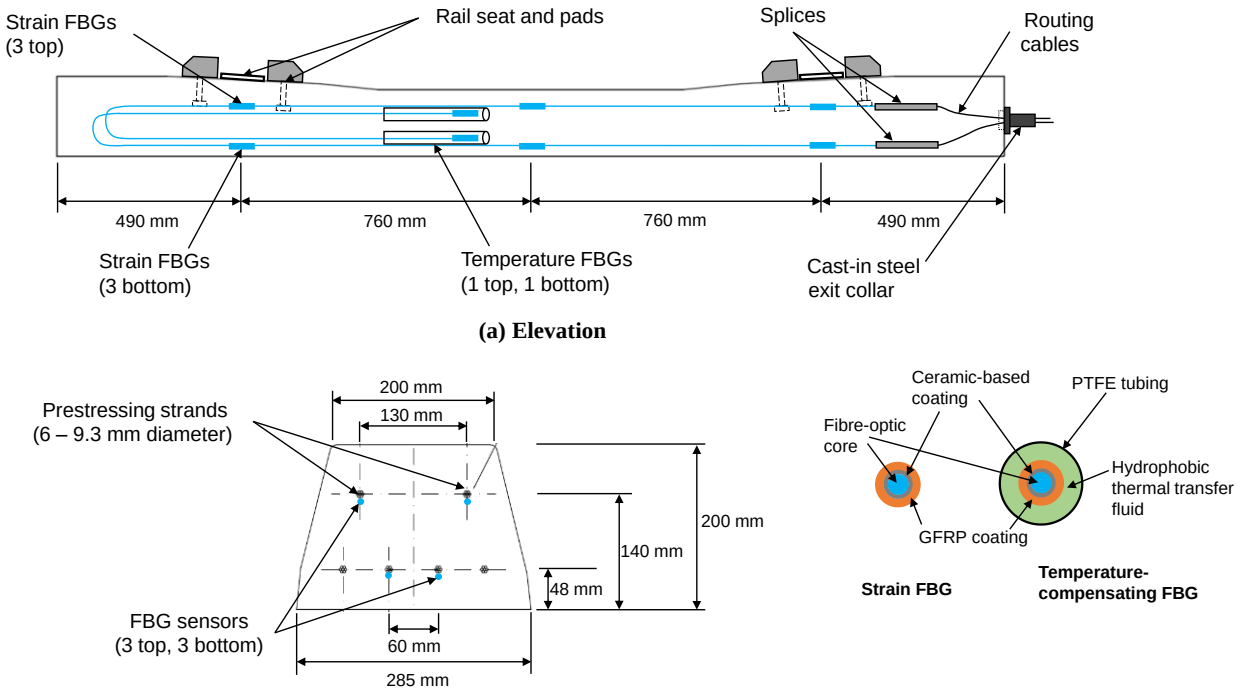

Figure 1. Sensor instrumentation and layout for typical self-sensing prestressed concrete sleeper

When strained, a FBG sensor measures a shift in its Bragg wavelength, which is linearly proportional to the strain and temperature change. In addition, the FBG wavelength shift is particularly affected by temperature [16], and therefore the installed temperature FBGs were used to compensate for strain changes due to temperature. The mechanical strain of an FBG stain sensor can be calculated by Equation 1 (adapted from [17]):

$$\Delta\varepsilon_M = \frac{1}{k_\varepsilon}\left[(\Delta\lambda/\lambda_0)_S - k_T\,(\Delta\lambda/\lambda_0)_T/k_{T_T}\right] - \alpha_{conc}\,(\Delta\lambda/\lambda_0)_T/k_{T_T} \quad (1)$$

Where,

$\Delta\varepsilon_M$= mechanical strain (compensated for all temperature effects);

$(\Delta\lambda/\lambda_0)_S$ = change in relative wavelength of strain sensor;

$(\Delta\lambda/\lambda_0)_T$ = change in relative wavelength of temperature compensating sensor;

k_ε = gage factor;

k_T = experimentally derived constant for temperature compensating sensor;

k_{T_T} = change of the refractive index of glass;

α_{conc} = linear coefficient of thermal expansion of concrete (/˚C).

This equation accounts for several effects: total (uncorrected) strain, strain measured from the temperature compensating sensors, and the thermal strain of the surrounding concrete. The calculated value is the mechanical strain produced by structural movements resulting from effects other than temperature. The fibre optic cable arrays were installed once the prestressing strands had been fully tensioned. The cables were fixed to the stands by a series of intermittently-spaced plastic cable ties and specially manufactured exit collars (see Figure 1a) were cast into the sleeper to protect the routing cables where they exited the sleeper. It was critical to devise a sensor installation method which was sufficiently robust, quick, and reliable in order to be readily incorporated into the sleeper production process without causing significant delay to CEMEX's operations. Once all of the cables were installed, they were plugged into the fibre optic analysers and tested sequentially prior to concrete casting. Figure 2 depicts the casting bays, the installed fibre optic sensors, and completed self-sensing sleepers.

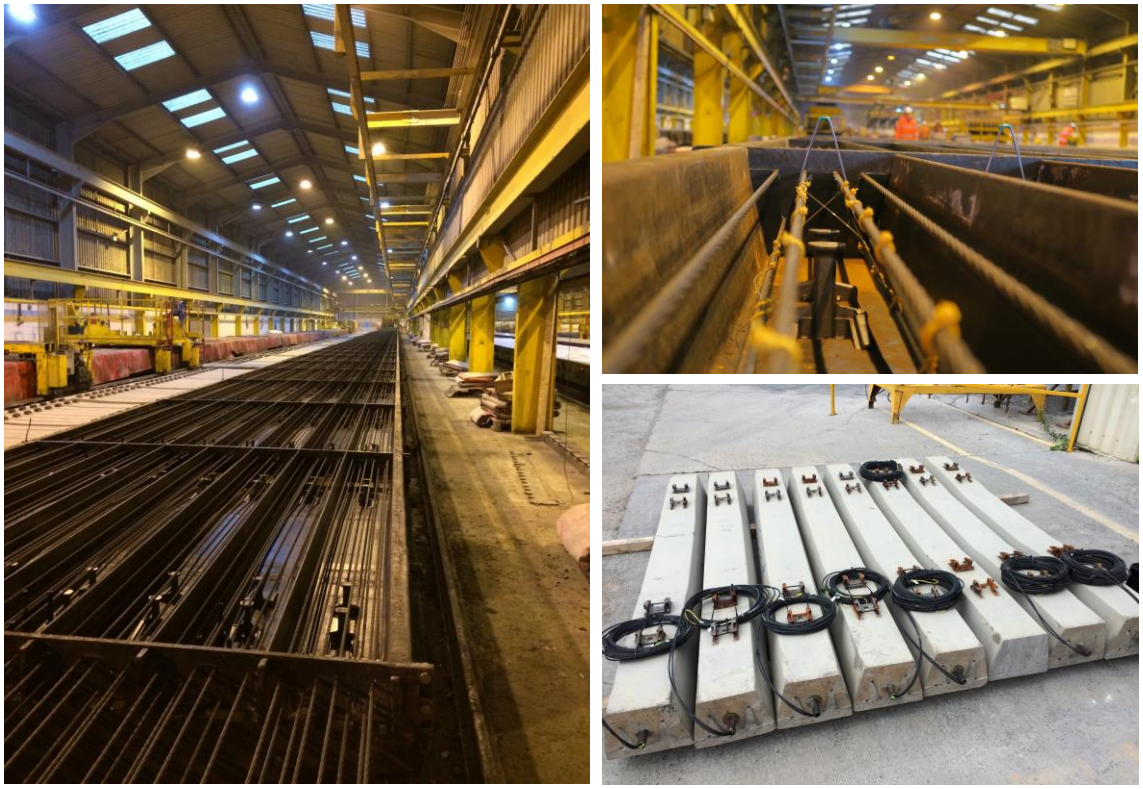

Figure 2. Sleeper production line and casting beds (left), sensor installation (top right) and completed Group 312 self-sensing sleepers (bottom right).

2.3 Monitoring programme

A total of twelve G44 type sleepers were manufactured in CEMEX UK over the course of several months. Eight sleepers were manufactured on July 20th 2015 (labelled as sleeper 312/1, 312/2, 312/3, 312/4, 312/5, 312/6, 312/7, and 312/8). These sleepers are herein referred to as Group 312. The other four sleepers (labelled as sleeper 360/1, 360/2, 360/7, and 360/8) were manufactured on November 17th 2015 and are referred to herein as Group 360. In terms of the manufacturing process and interior facility conditions, there was little difference between both sleeper groups. An overview of the experimental programme is shown in Table 1.

Table 1. Overview of experimental and monitoring programme

Stage		Group 312 sleepers		Group 360 sleepers	
		Date	Sleeper no.	Date	Sleeper no.
Manufacturing*	Casting	20/07/2015	312/1, 312/2, 312/3, 312/4, 312/5, 312/6, 312/7, 312/8	17/11/2015	360/1, 360/2, 360/7, 360/8
	Curing	20/07/2015-21/07/2015		17/11/2015-18/11/2015	
	Detensioning	21/07/2015		18/11/2015	
Rail seat bending qualification testing		21/07/2015	312/8	18/11/2015	360/7
†Temporary storage up until transport to site		21/07/2015-18/11/2015	312/1,2,3, 4,5,6,7,8	18/11/2015-Present‡ Awaiting future lab testing	360/1,2,7,8

*Strain readings were recorded for sleepers 312/6, 8 in Group 312 and all sleepers in Group 360.
†Strain readings were recorded on 18/11/2015 for all eight Group 312 sleepers.
‡In-storage strain readings for sleeper group 360 are scheduled at a later date prior to future laboratory testing.

3.0 Results and analysis

3.1 Material properties

To provide better estimates of sleeper behaviour and prestress loss, a variety of concrete and prestressing steel material properties were measured as part of this research. In addition, detailed records of the curing, detensioning and storage procedures were also used for understanding sleeper performance variability. Table 2 presents the measured concrete and prestressing steel material properties for both sleeper groups.

Estimates of concrete elastic modulus at the time of prestress transfer (approximately 1 day) and at 28 days were calculated using Eurocode 2 formulae and the measured compressive strengths [18]. It is important to note that the concrete mixture designs and curing procedures for both sleeper groups were identical; however, it is evident from Table 2 that the concrete strength values were considerably different. Although both concrete mixtures had a target w/c ratio of 0.32, it is hypothesized that Group 360 sleepers had a slightly higher w/c ratio as evidenced by the higher slump flow. A higher w/c ratio may explain the lower compressive strength in Group 360 sleepers.

Table 2. Material properties for sleeper groups 312 and 360

Material property	Group 312	Group 360
Concrete		
Casting date	20 Jul. 2015	17 Nov. 2015
Target water/cement (w/c) ratio	0.32	0.32
Cement strength class as per Eurocode 2	Class R[1]	Class R[1]
Slump flow	710 mm	760 mm
Design f_{ck} (28 days)	60 MPa	60 MPa
$f_{ck,meas,cube}$ (28 days)[2]	93.6 MPa	79.2 MPa[5]
$f_{ck,meas,cube}$ at transfer (1 day)[2]	42.7 MPa	35.9 MPa
Estimated E_{cm} at transfer[3]	31820 MPa	30190 MPa
Estimated E_{cm} at 28 days[3]	40250 MPa	38290 MPa
Prestressing steel (9.3 mm dia. 7 wire strand)	6 strands	6 strands
Tension per strand prior to transfer	69.0 kN	68.8 kN[4]
f_{pu}[6]	1770 MPa	1770 MPa
E_p[6]	195 000 MPa	195 000 MPa
Strand cross-sectional area	52 mm^2	52 mm^2

[1] High early strength gain
[2] Measured values are based on 100 mm cube specimens cured under controlled conditions, i.e. in water bath. Target strength for detensioning was 35 MPa. Also note the assumption that measured values of compressive strength, $f_{c,meas,cube}(t) = 0.8(f_{ck}(t) + 8) = 0.8f_{cm}(t)$
[3] $E_{cm}(28)=22(f_{cm}(28)/10)^{0.3}$; $(E_{cm}(1) = (f_{cm}(1)/f_{cm}(28))^{0.3}E_{cm}(28)$; $f_{ck}(t) = 0.8f_{ck,cube}(t)$
[4] Measured by pre-casting facility operators immediately prior to detensioning.
[5] Interpolated based on 21 day and 49 day results.
[6] Based on supplier specifications sheets.

3.2 Manufacturing process monitoring

Once the FBG sensors were attached to the prestressing strands, they were plugged into the fibre optic analysers for testing. It was noticed that several sensors were malfunctioning; however, due to the high-paced nature of the sleeper production process, it was not possible to carry-out repairs. Sleepers 312/6 and 312/8 in Group 312 and all Group 360 sleepers were monitored simultaneously during the entire manufacturing process.

Figure 3 presents the monitoring results for sleeper 312/8 to provide an overview of the strain developed during the manufacturing process (casting, curing and detensioning). It can be seen that the FBG sensors captured the strain change during the entire process. The top and bottom strains differ due to the change in sleeper cross-section along its length, different number of strands, and eccentricity between the prestressing steel centroid and the centroid of the concrete section. In discussing the strain changes during manufacturing, the strain

baseline was taken as the strains recorded at one hour after casting in order to allow sufficient bond to develop between the prestressing strands, the installed sensor cables, and the concrete.

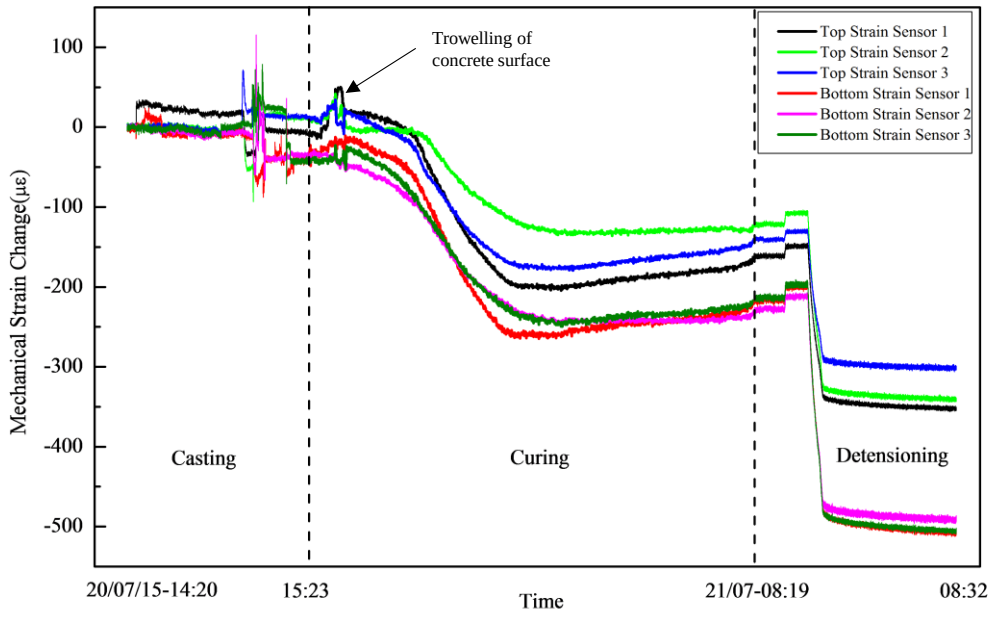

Figure 3. Typical mechanical strain change during the entire manufacturing process for sleeper 312/8 (time axis not to scale)

3.2.1 Curing stage

Figure 4 shows the mechanical strain change during curing for both sleeper groups. Each sleeper displayed a similar trend during concrete curing: a significant increase in compressive strain (shrinkage) during the first 6 to 8 hours followed by a plateau with no significant strain change for 3 to 4 hours, then finally, a gradual increase in strain (expansion) just prior to detensioning. A wide range of strains between the start and end of the curing period was also observed among the various sleepers monitored. In addition, strain change (due to shrinkage) during curing appeared to be highly non-uniform along the length and depth of the sleepers. There appeared to be no clear trend between the strain change measured in the top and bottom sensors. Given that the sleepers were covered with plastic sheathing (to avoid excess moisture loss), this would explain why the top of the sleepers did not necessarily experience higher shrinkage than the bottom. Based on the general observed strain change trends (i.e.

initial development of compression) observed in each sleeper, it appears that one of the top sensors in sleeper 312/6 (top strain sensor 1) was malfunctioning during this monitoring stage. On average, Group 360 sleepers experienced higher strain changes as compared with Group 312 sleepers. This may be due to differences in the effective w/c ratio as previously discussed. A higher w/c ratio indicates a higher water content which may result in higher shrinkage strains and lower compressive strength (refer to Table 2).

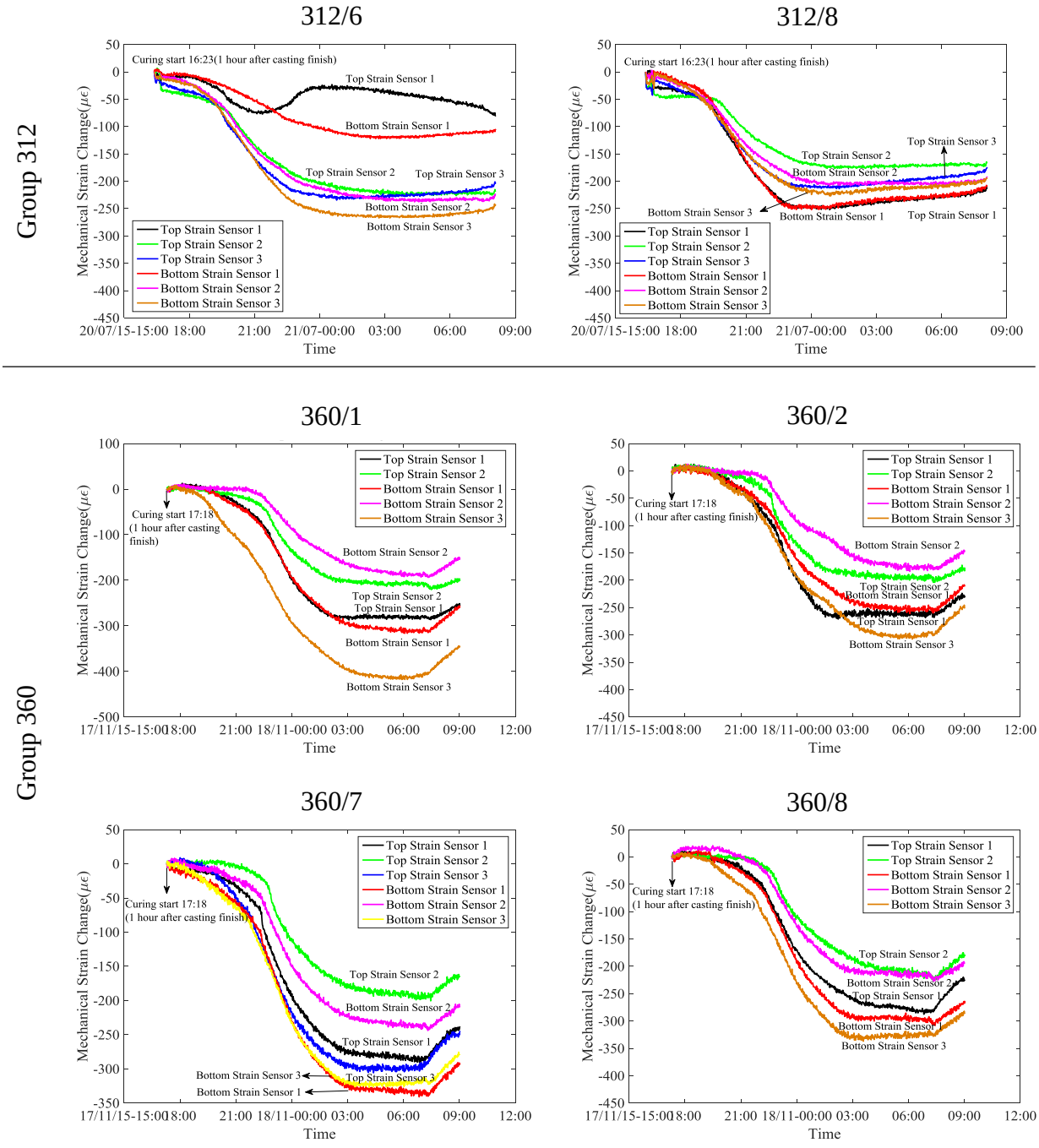

Figure 4. Mechanical strain change during concrete curing

As described in Section 4, temperature significantly affects the FBG wavelength shift and therefore, precise strain results can only be acquired by properly compensating for temperature. In addition, the concrete and prestressing tendons may also undergo strain changes due to temperature (thermal strain) and this effect needs to also be considered in the calculation of the mechanical strain (in the case of concrete and steel, both are assumed to experience similar strain changes due to temperature). It is particularly important when monitoring concrete curing to measure strain change due to temperature as the hydration process is an exothermic reaction. In general, the strain development and corresponding transfer of strain to the prestressing strands is a highly complex process. Carlsson (2012) determined various factors including rate of temperature development during hydration (which in turn affects bond development), ambient temperature variation, total casting time, and time-dependent variation of coefficient of thermal expansion that all influence the strain changes during the curing period prior to detensioning [3].

3.2.2 Detensioning stage

After curing overnight for approximately 18 hours, the concrete (in both sleeper groups) had achieved adequate strength and the prestressing strands were detensioned and subsequently cut. Figure 5 shows the mechanical strain change for both sleeper groups during detensioning. A slight increase in positive strain in both groups occurred prior to detensioning which is the result of an additional tensile force being introduced in order to release the hydraulic jacking clamps. A sharp decrease in strain (compression) is observed followed by nearly constant strain region after the strands were cut.

In the majority of the sleepers, a distinct difference in top and bottom strains was measured. This difference in strain between top and bottom of the sleeper translates to a curvature change causing a net upwards deflection or camber. There was an abrupt (positive) jump in strain recorded for Group 360 sleepers after detensioning which was a result of the strand

cutting process. Note that as indicated in Figure 5, bottom strain sensor 1 in sleeper 312/6 began to malfunction during the detensioning process as it recorded only zero strain.

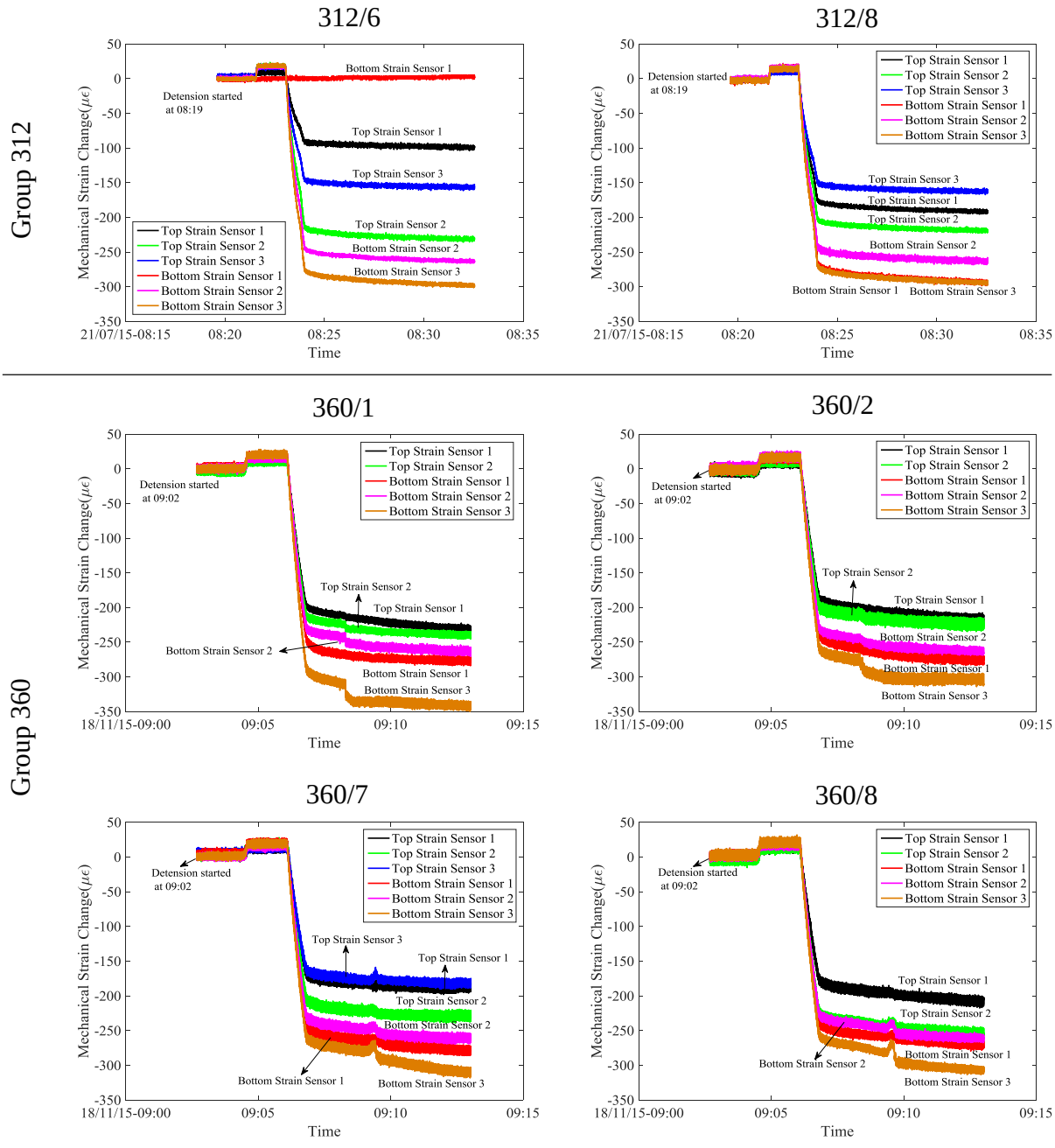

Figure 5. Mechanical strain change during detensioning of prestressing strands

The overall level of noise in the recorded data was nearly twice as high for Group 360 sleepers compared with that for Group 312 sleepers (±10με for Group 360 versus ±5με for Group 312). This difference in measurement noise is believed to be the result of the signal multiplexing. The two Group 312 sleepers were monitored using a four channel fibre optic

analyser (2 channels per sleeper) whereas the four Group 360 sleepers were monitored using the same 4-channel fibre optic analyser in combination with a 16-channel multiplexer. Using a multiplexer has the effect of reducing the maximum sampling frequency by a factor of four (i.e., from 1000 Hz to 250 Hz), and it also appears to increase the sampling noise by a factor of two.

3.2.3 Assessment of performance variability during production

To begin to investigate the effects that the production process has on the internal strain change within the sleepers, the average strain changes (average of top and bottom sensor readings) that were measured during the curing and detensioning stages are summarised in Figure 6. These average top and bottom strains were then used to interpolate the average strain change at the centroid of the prestressing strands (CPS). It is also important to note that the strain change in each stage is based on the strain state at the end of the previous stage (i.e., they are not cumulative).

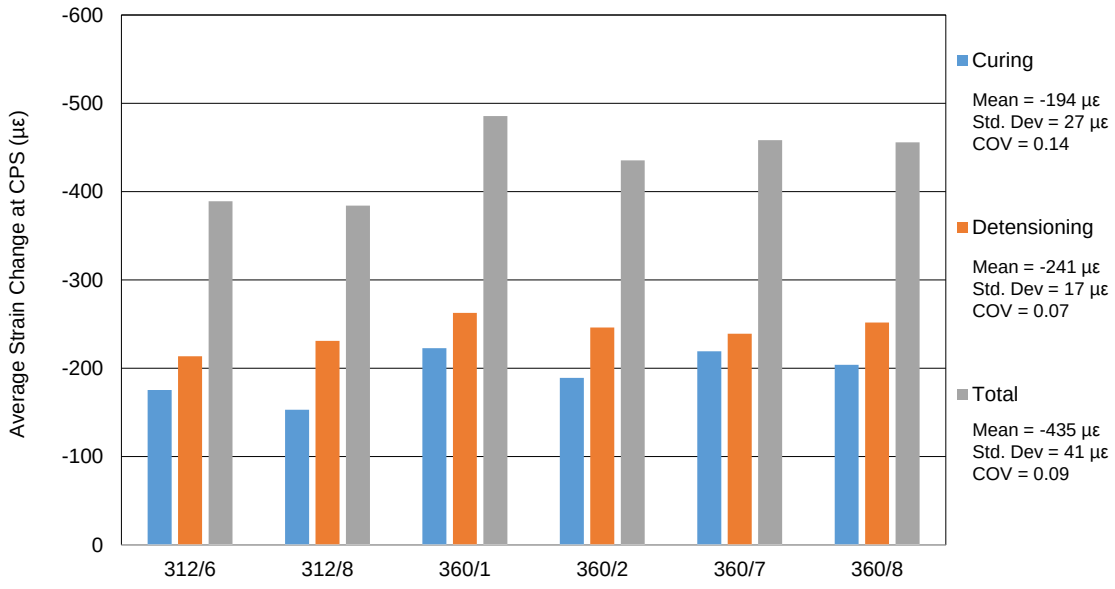

Figure 6. Mechanical strain change during manufacturing stages

It appears that the strain changes were most variable during the curing stage (COV = 0.14) whereas the variability during the detensioning stage was significantly lower (COV = 0.07). In general, Group 360 sleepers underwent total strain changes during the manufacturing

process that were 16% higher compared to those experienced by Group 312 sleepers. This difference in strain appears to primarily be the result of higher strain changes during the curing of Group 360 sleepers which may be a result of the difference in concrete strengths and ambient conditions (i.e. relative humidity).

3.3 Rail seat bending qualification test

As part of CEMEX's quality control programme, a select number of sleepers are required to undergo routine bending tests in accordance with BS EN 13230-2-2009 [19]. In this experimental study, sleepers 312/8 and 360/7 were selected to undergo static rail seat positive bending testing. The tests were carried out approximately 24 hours after casting. The test setup, loading regime, and a photograph of testing in progress are presented in Figure 7. The sleepers in this study had an initial reference load, F_{r0}, of 223 kN. This load was then held constant for a period of 10 seconds before increasing (by 2 kN/s) up to a load which caused the first crack in the bottom section, F_{rr}. If $F_{rr} > F_{r0}$, the sleeper is deemed to be fit for service. A value of F_{rr} was recorded for each sleeper tested before the loading was removed.

The top and bottom strain behaviour for sleepers 312/8 and 360/7 during the rail seat bending qualification test were captured and are presented in Figure 8. Sleeper 312/8 reached the initial reference load of 223 kN with no signs of cracking (corresponding top and bottom strains were -210 με and 200 με, respectively). Both the top and bottom FBG sensors registered strains that remained linear with time up to the constant strain plateau. On further loading, the first bottom crack was observed at a load of 298 kN. Beyond the constant strain plateau, the strain response became increasingly non-linear indicating the onset of microcracking in the concrete. Therefore, sleeper 312/8 passed the test as $F_{rr} > F_{r0}$; however, residual strain was induced in the sleeper after the test was completed.

Note that the test procedure for sleeper 360/7 was slightly modified in order to use the FBG sensors to study the effects of cyclic loading and unloading on the sleeper. Sleeper 360/7 was subjected to three loading cycles where it was loaded up to the reference load F_{r0} = 223 kN and then unloaded. This was followed by a fourth cycle where it was loaded up to F_{r0} and then additionally loaded up until the first crack was observed at F_{rr}.

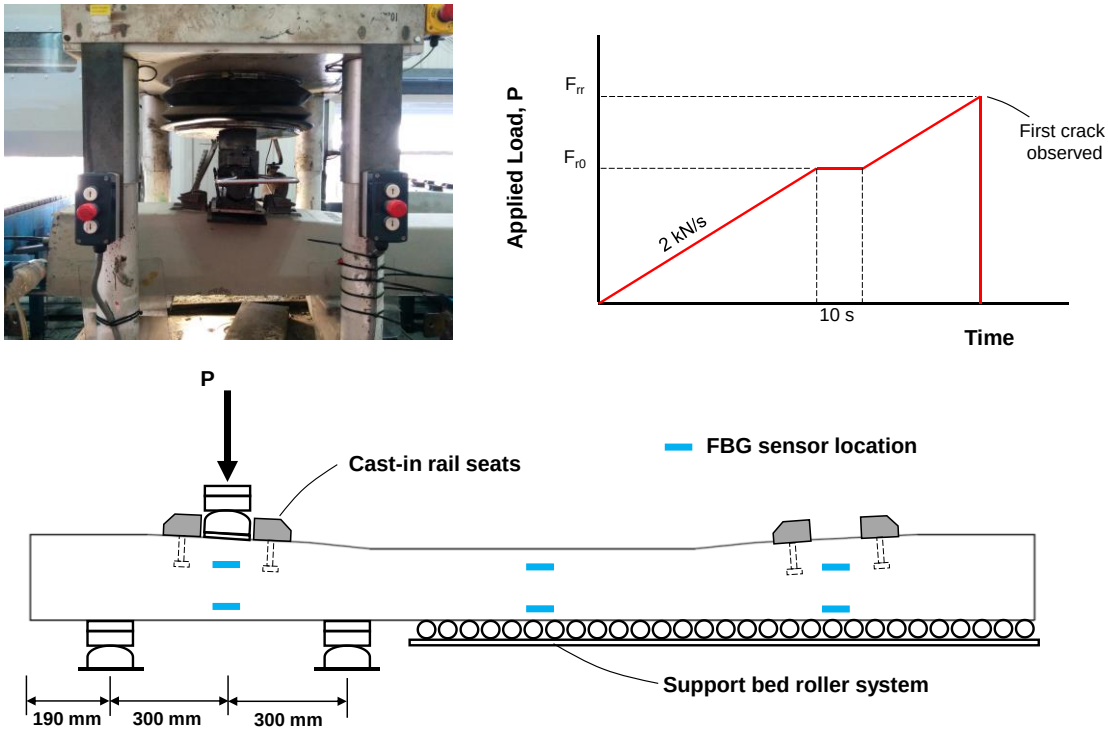

Figure 7. Static rail seat positive bending test setup

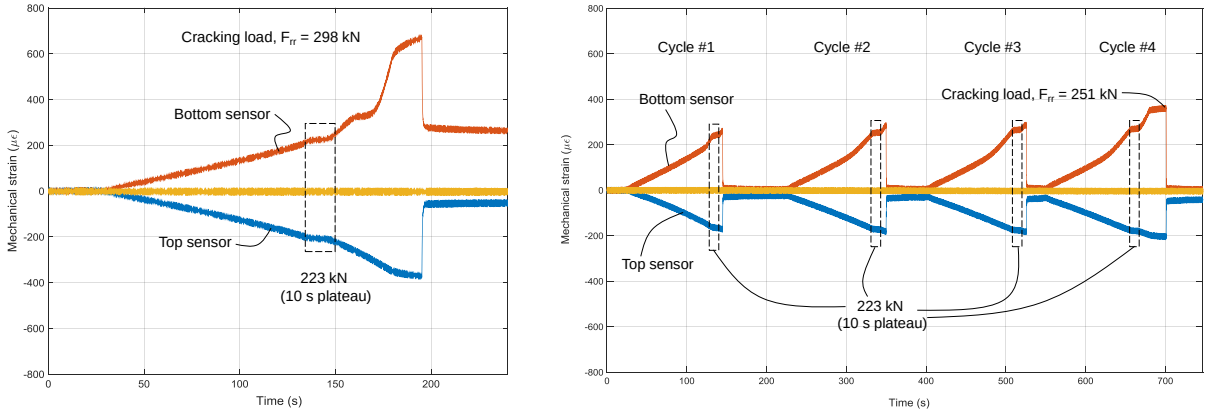

(a) **(b)**

Figure 8. Mechanical strain response at the rail seat section for (a) sleeper 312/8 and (b) sleeper 360/7

Similar strain change values were observed in the first three cycles. The first crack was observed at a load of 251 kN (corresponding to maximum measured strains of 370 με and -210 με in the bottom and top sensors, respectively). This load was 16% lower than the cracking load reached by sleeper 312/8 (298 kN). This difference is most likely due to the differences in measured concrete strengths (and associated flexural and tensile strengths) at the time of testing (refer to Table 2). As load cycles progressed, the bottom sensor captured the increasingly non-linear strain response caused by an increase in internal microcracking in the concrete with every load cycle. Therefore, the FBG sensor results seem to suggest that it might be inappropriate to define 'first cracking' as the first observable crack but rather as the first observable sign of non-linearity in the load-strain response.

3.4 Strain change during temporary storage period

Group 312 sleepers were stored for approximately four months prior to being transported to site and strain changes were recorded for all eight sleepers. Strain changes within this period mainly result from early age concrete creep, shrinkage, and steel relaxation. Figure 9 presents the average measured strain change for Group 312 sleepers during the temporary storage period. Similar to strain changes during manufacturing, the average top and bottom strains were used to interpolate the average strain change at the centroid of the prestressing strands (CPS).

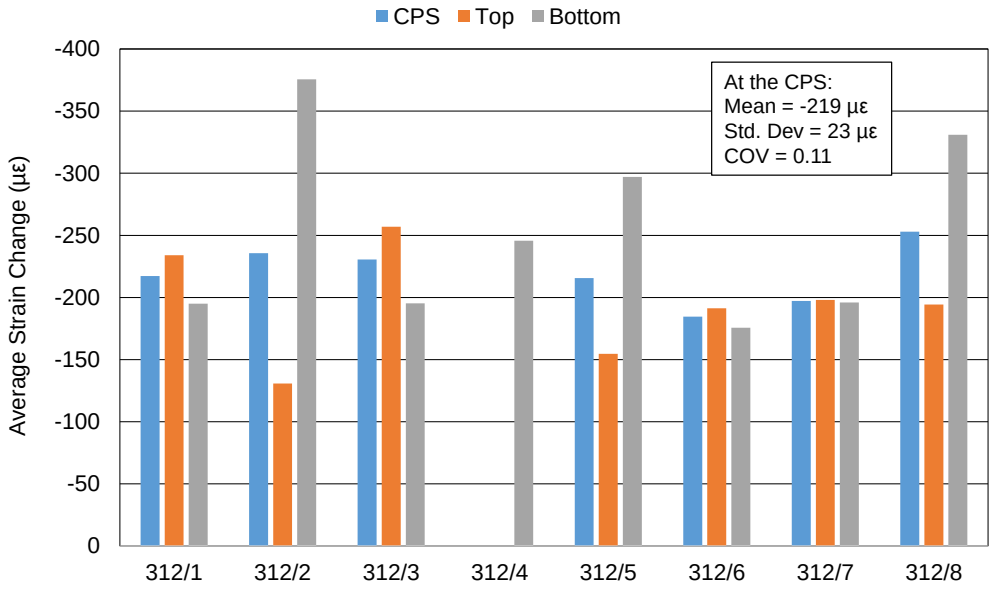

Figure 9. Average measured strain change during temporary storage period

Early age storage results are not presented for Group 360 sleepers as they have continued to be stored and will be undergoing additional full-scale testing in the future. Note also several of the top sensors malfunctioned for sleeper 312/4 and therefore, results are not included. Overall, a variation in average strain between -185 με and -253 με took place during the storage period for Group 312 sleepers. This translated to a slightly higher coefficient of variation as compared to the strain changes that occurred during the manufacturing process.

3.5 Prestress loss predictions and measurements

The behaviour of prestressed concrete members are highly time-dependent and, as a result, the effective prestressing force within the tendons varies with time. Estimation of prestress losses at various construction and loading stages is a critical exercise for ensuring that prestressed concrete members perform adequately under serviceability conditions. The accurate estimation of prestress losses can be highly complex as a variety of material and environmental factors contribute to the time-dependent behaviour of prestressed concrete. Namely, effects such as steel relaxation, elastic shortening of concrete, shrinkage and creep

all work inter-dependently to reduce the effective amount of prestress within a structural member over time.

Prestress losses were calculated based on the provisions of Eurocode 2 equations [18] summarised in Table 3. Note that prestress loss values were calculated at several discrete time steps corresponding to when fibre optic sensor measurements were taken. In the calculation of the shrinkage strain and creep coefficient, a constant relative humidity value of 70% was assumed as recommended for the design of concrete members in the UK [20]. In addition, the effect of surface area on concrete shrinkage was considered in the calculation of the notional size of the cross-section, $h_o = 2A_c/L$, where A_c is the cross-sectional area and L is the length of the cross-section perimeter exposed to drying [20].

Prior to the transfer of prestress, a significant amount of autogenous shrinkage occurs during concrete hydration and subsequent curing. It occurs as a result of the free water moving out of the pores due to the hydration reaction in concrete [21]. The total long term shrinkage of concrete is split into two components: autogenous shrinkage and drying shrinkage. The autogenous component occurs relatively quickly as it reaches the majority of its completion within the first 3 to 4 months following casting [21]. Given that the curing period of the prestressed sleepers is relatively short and the w/c ratios of the concrete mixtures are relatively low (as is typical in high-strength concrete), a large proportion of the autogenous shrinkage is expected to occur prior to the release of prestress [22]. Therefore, the prestress losses due to autogenous shrinkage were included in the prestress loss predictions presented in Table 4.

Table 3 Summary of Eurocode formulae for calculating prestress losses

Source of prestress loss	Eurocode 2 Formulae
Steel relaxation	$\Delta P_{REL,i}=6.6A_p(\sigma_{pi})\rho_{1000}e^{9.1\mu}\left(\frac{t}{1000}\right)^{0.75(1-\mu)}\times10^{-6}$
Autogenous shrinkage	$\varepsilon_{ca}(t)=\beta_{as}(t)\varepsilon_{ca}(\infty)$ $\varepsilon_{ca}(\infty)=2.5(f_{ck}-10)\times10^{-6}$ $\beta_{as}(t)=1-\exp(-0.2t^{-0.5})$
Elastic shortening	$\Delta P_{ES}(t)=\frac{A_p\frac{E_p}{E_{cm}(t)}\sigma_c}{1+\frac{E_p}{E_{cm}(t)}\frac{A_p}{A_c}\left(1+\frac{A_c}{I_c}e^2\right)}$
Time-dependent creep, shrinkage and steel relaxation	$\Delta P(t)_{C+S+R}=A_p\Delta\sigma_{p,c+s+r}$ $=A_p\frac{\varepsilon_{cs}E_p+0.8\Delta\sigma_{pr}+\frac{E_p}{E_{cm}}\varphi(t,t_0)\sigma_{c,qp}}{1+\frac{E_p}{E_{cm}}\frac{A_p}{A_c}\left(1+\frac{A_c}{I_c}e_{cp}^2\right)[1+0.8\varphi(t,t_0)]}$
Total prestress losses	$\Delta P_{TOT}=\Delta P_{REL,i}+\Delta P_{ES,i}+\Delta P_{C+S+R}$ $\%\text{Loss}=\Delta P_{TOT}/\Delta P_i$

As indicated in Table 4, both sleeper groups are predicted to have similar levels of instantaneous losses. Group 360 is predicted to have slightly higher long term (50 years) losses compared to Group 312 sleepers primarily due to higher levels of concrete shrinkage and creep resulting from their lower compressive strength. In the case of Group 312 sleepers, they are predicted to undergo 79% of their total prestress losses by the time they are installed (119 days after casting).

Table 4. Predicted prestress losses for Group 312 and 360 sleepers

	Group 312		Group 360	
Time Stage	Δσp [MPa]	Δσp/σpi ×100%	Δσp [MPa]	Δσp/σpi ×100%
Losses due to early steel relaxation and autogenous shrinkage††	15.2	1.1%	15.6	1.2%
Transfer of prestress*	53.0	4.0%	55.7	4.2%
Total instantaneous losses	**68.2**	**5.1%**	**71.3**	**5.4%**
After installation (119 days after casting)†	197.6	13.5%	N/A	N/A
Final long term losses (50 years)	**251.4**	**18.9%**	**292.8**	**22.1%**

Note: σ_{pi} = 1327 MPa (approximately 75% of f_{pu})
†† Autogenous shrinkage was accounted for in the early stages prior to detensioning.
* Calculation accounts for tendon relaxation losses prior to detensioning.
† Includes all instantaneous losses, i.e. cumulative losses.
Refer to Table 2 for concrete materials properties.

Using the mechanical strains measured by the fibre optic sensors, the strain changes within the prestressing strands were calculated to provide an estimate of the loss of prestress. Based on the installation procedures adopted, the sensors were installed within the concrete but directly adjacent to the prestressing tendons. A primary assumption is that there is perfect bond between the prestressing tendon and the surrounding concrete and that the strain in the concrete directly in contact with the steel (at any given point along the strand) is equal to the strain in the steel at that point. In this way, prestress losses (based on the measured strain results) was calculated using equation 4,

$$\%\text{Loss} = \frac{\Delta\sigma_p}{\sigma_{pi}} \times 100\% = \frac{\Delta\varepsilon_{m,cps} E_p}{\sigma_{pi}} \times 100\% \quad (4)$$

where, $\varepsilon_{m,cps}$ is the mechanical strain at the centroid of the prestressing steel interpolated from the measured top and bottom strains, E_p is the elastic modulus of the prestressing strands , and σ_{pi} is the initial level of prestress before any losses have occurred (refer to Table 2 for

material properties). A comparison between the FBG measured and Eurocode predicted prestress losses is presented in Table 5.

Table 5. Comparison between FBG measured and Eurocode predicted prestress losses

	Group 312 Sleepers		Group 360 Sleepers			
	312/6 Loss *(Δσ, MPa)* **Meas/Pred**	312/8 Loss *(Δσ, MPa)* **Meas/Pred**	360/1 Loss *(Δσ, MPa)* **Meas/Pred**	360/2 Loss *(Δσ, MPa)* **Meas/Pred**	360/7 Loss *(Δσ, MPa)* **Meas/Pred**	360/8 Loss *(Δσ, MPa)* **Meas/Pred**
Pre-detensioning and curing	2.5% *(32.9)* **2.16**	2.1% *(27.4)* **1.80**	2.5% *(33.7)* **2.16**	1.6% *(21.4)* **1.37**	2.8% *(37.8)* **2.42**	2.5% *(32.7)* **2.10**
Transfer of prestress	3.4% *(44.9)* **0.85**	3.6% *(47.7)* **0.90**	4.0% *(52.9)* **0.95**	3.8% *(49.8)* **0.89**	3.7% *(48.9)* **0.88**	3.8% *(50.5)* **0.91**
Total Instantaneous losses	5.9% *(77.8)* **1.14**	5.7% *(75.1)* **1.10**	6.5% *(86.6)* **1.21**	5.4% *(71.2)* **1.00**	6.5% *(86.7)* **1.22**	6.3% *(83.2)* **1.17**
After rail seat bending test	N/A	5.7% *(75.1)*†	N/A	N/A	6.8% *(89.6)*	N/A
119 days after casting*	8.6% *(113.8)* **0.57**	9.4% *(124.4)* **0.63**	Still in storage and awaiting future lab testing			
% of EC2 predicted final long term losses (50 years)	**45%**	**49%**				

Note: predicted values are those based on the Eurocode 2 equations presented in Section 7.1.

† Following the bending test there was a measured increase in the strain at the centroid of the strands; however, this cannot add to the amount of prestress in the strand and therefore, no net change in the effective prestress was assumed to occur during the bending test.

* Measured strain data for sleepers 312/1, 312/2, 312/3, 312/4, 312/5, and 312/7 during their temporary storage were also recorded with a mean prestress loss of 42.7 MPa.

Based on Table 5, the measured prestress loss values due to transfer of prestress closely match those predicted using the Eurocode 2 equations (refer to Table 4). However, the losses predicted to occur prior to the transfer of prestress greatly underestimate the measured values by up to 242% (sleeper 360/2). Carlsson (2012) reported comparable findings when they compared measured losses prior to detensioning of sleepers produced in two different factories [3]. One reason for this may be that the strain due to autogenous shrinkage that occurs during the early stages of concrete hydration and curing is higher than that predicted by the Eurocode 2 equations. Carlsson (2012) suggested that the surrounding ambient

temperatures may have accounted for these differences. Another possible explanation involves the time-dependent nature of bond development between the prestressing strands and the concrete. If the time required for sufficient bond to occur between the concrete and the sensor cable is less than that required between the concrete and the prestressing steel, the fibre optic sensors will start to measure shrinkage strains occurring within the concrete before they are fully transferred to the steel (and thus inducing a loss of prestress) [23].

The strain changes measured by the sensing system during the temporary storage period was significant and resulted from concrete shrinkage, creep and steel relaxation. However, the FBG-measured prestress loss values at the end of this period were still significantly lower compared with the Eurocode-predicted values. These results indicate that the creep, shrinkage and relaxation (time-dependent prestressed concrete properties) were lower than those predicted by the code equations. Based on the sensor-measured prestress loss values, sleepers 312/6 and 312/8 had experienced 45% and 49% of the long-term (Eurocode 2) predicted values within the first four months after manufacture, respectively. Therefore, the sensor results have revealed that the overall performance of the sleepers appears to be within acceptable design limits prior to being placed in-service.

4.0 Finite element modelling

In addition to the data analysis presented above, a 3D non-linear finite element (FE) model was constructed to provide additional insight into the early-age (pre-service) behaviour of prestressed concrete sleepers.

4.1 FE model description

The prestressed concrete sleeper FE model was built using Diana 10.0. As shown in Figure 10, the geometry profile of the model was defined based on a G44 type sleeper (refer to Figure 1). The cross-sectional area of the prestressed strands was defined as an equivalent

circular area (refer to Figure 10(a)). The concrete was modelled using an eight-node isoparametric solid brick element (HX24L) and the prestressing strands were modelled using an embedded reinforcement element (BAR). Additional element information is provided in the DIANA documentation manual [24]. The concrete and prestressing strands were assumed to be perfectly bonded. The prestressing force was applied via an initial stress in the BAR element equivalent to the prestressing force measured during the manufacturing process (refer to Table 2).

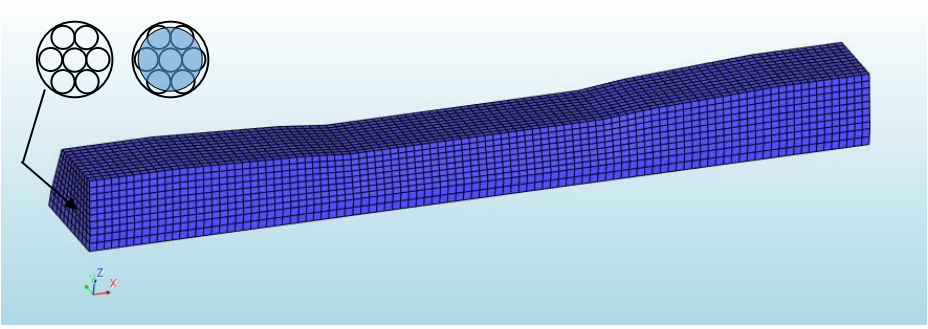

(a) Geometry profile and meshing

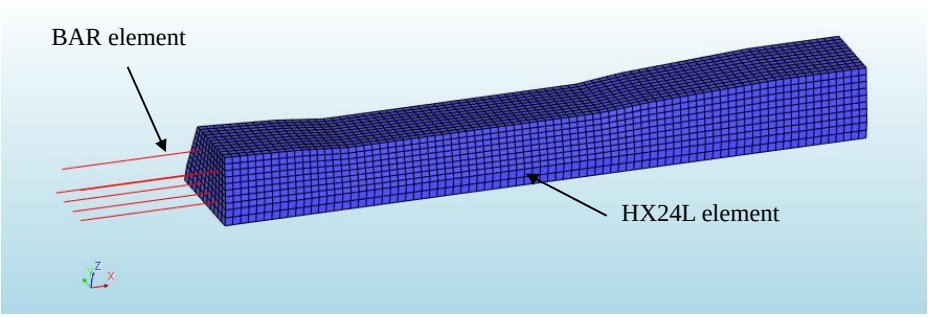

(b) Element types and assignments

Figure 10. Finite element model of the prestressed concrete sleeper

The behaviour of concrete in compression was modelled using Eurocode 2 recommended nonlinear constitutive relationship. Concrete in tension was assumed to behave linearly elastically up until the specified tensile strength was reached. When strains exceeded the tensile limit, a multi-directional fixed crack model with a nonlinear tensile softening relationship was used to simulate the cracked concrete response. The concrete compressive strength at one day, $f_{cm}(1)$ (i.e. the time of transfer of prestress), and 28 days, f_{cm}, were based

on the measured properties presented in Table 2. The elastic modulus at one day and at 28 days and the tensile strength, f_{ctm}, at one day were calculated according to Eurocode 2 EN 1992-1-1 [19]. The material model for the prestressing steel strands was based on a two-part idealized elastoplastic relationship with an elastic modulus, E_s, of 195 GPa and tensile strength, f_{pu}, of 1770 MPa.

4.2 FE simulation of detensioning process and bending qualification test

The detensioning process of sleeper 312/8 was simulated by applying an initial stress to the BAR elements. The measured tensile force for each prestressed strand was 69 kN with a corresponding stress value of 1327 MPa. According to the measured values of strain change presented in Table 5, there was 2.1% loss of prestress prior to detensioning; therefore, a stress value of 1299 MPa was applied to the prestressing strands (BAR elements). The FE analysis results of the stress distribution of the sleeper due to the transfer of prestress (detensioning) are shown in Figure 11a. Stress concentrations were present at the ends of the sleeper surrounding the prestressing strands. Away from the end regions, the FE model showed that concrete experienced compression due to the transfer of prestress that ranged between -6 MPa and -11.2 MPa. The FE-predicted stress distribution was non-uniform along the length and depth of the sleeper due to changes in the sleeper geometry. The compressive stress (and corresponding strain) at the bottom of the sleeper was higher than that at the top. A comparison between the FE-predicted and FBG-measured strain change along the sleeper length due to detensioning is shown in Figure 11b. At the top FBG locations, the measured stress change in the middle region is higher than that at the rail seat locations, which is consistent with the FE-calculated results. At the bottom FBG locations, the FE-calculated strain change is constant along the length of the sleeper whereas the measurement results show non-uniform strains along the length of the sleeper. These differences may be attributed to the heterogeneous nature of concrete which is difficult to account for using a homogeneous

FE model and in the estimation of the concrete stiffness using compressive strength test results. The friction generated between the concrete and the steel sleeper mould during detensioning may have also contributed to the slightly larger FE model generated strains as compared to the FOS measured strains.

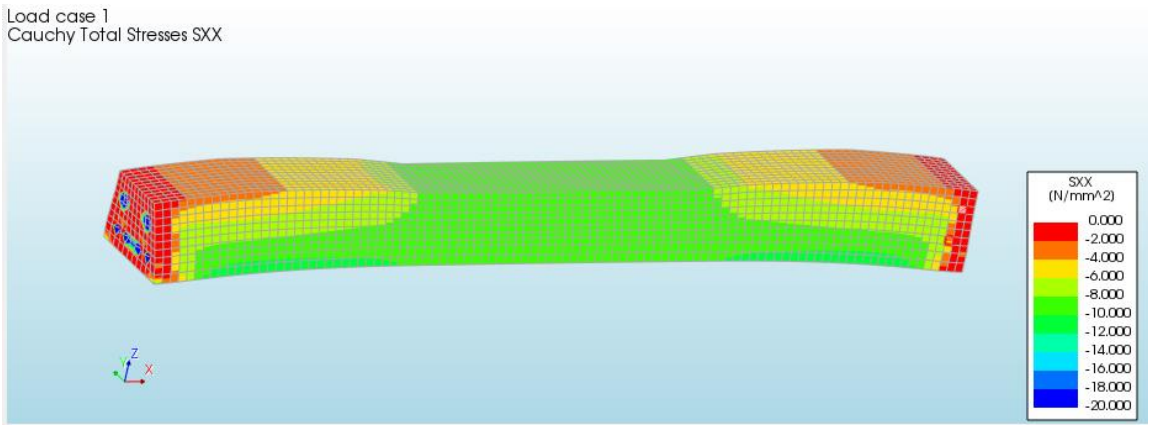

(a) FE stress distribution

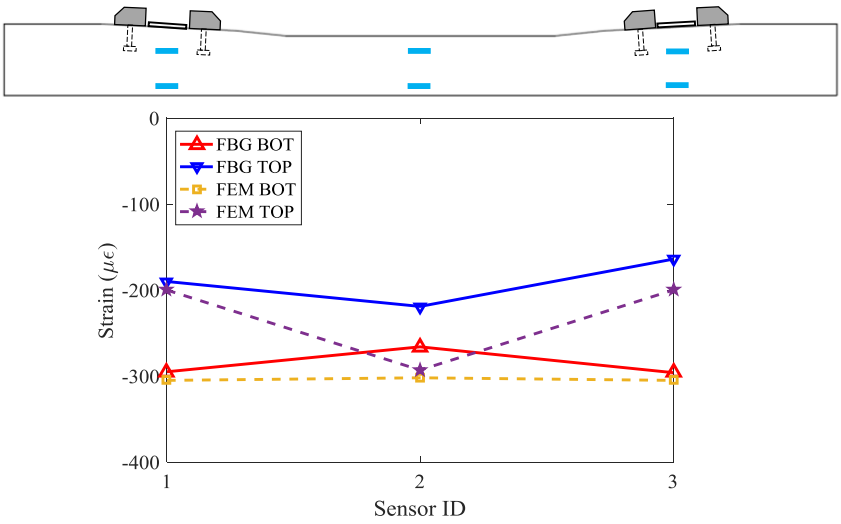

(b) Measured and FE strain distribution

Figure 11. Sleeper FE analysis results and comparison with measured FBG sensor strains of sleeper 312/8 due to the detensioning process.

The next step of FE modelling involved simulating the strain change at the FBG sensors' location during the rail seat bending qualification test of sleepers 312/8 and 360/7. The applied load was consistent with the loading regime used in the bending tests. Both the FBG

measured and FE predicted strain versus applied load relationships are presented in Figure 12.

The FE results for sleeper 312/8 closely match the FBG results. However, while the FE results for sleeper 360/7 display a similar trend in response, deviations from the measured response mainly arise due to inaccurate estimates of early-age concrete properties. A series of parametric studies were performed in order to determine the values of elastic modulus and tensile strength that would provide the best fit to the actual measured response. The early-age concrete properties were modified by decreasing both the Eurocode-calculated concrete elastic modulus and tensile strength by approximately 12% and 16% respectively. The modified FE results for sleeper 360/7 provided a better estimate of the experimental results. This implies that the Eurocode equations may have slightly overestimated the elastic modulus and tensile strength for the early-age concrete model used in this case.

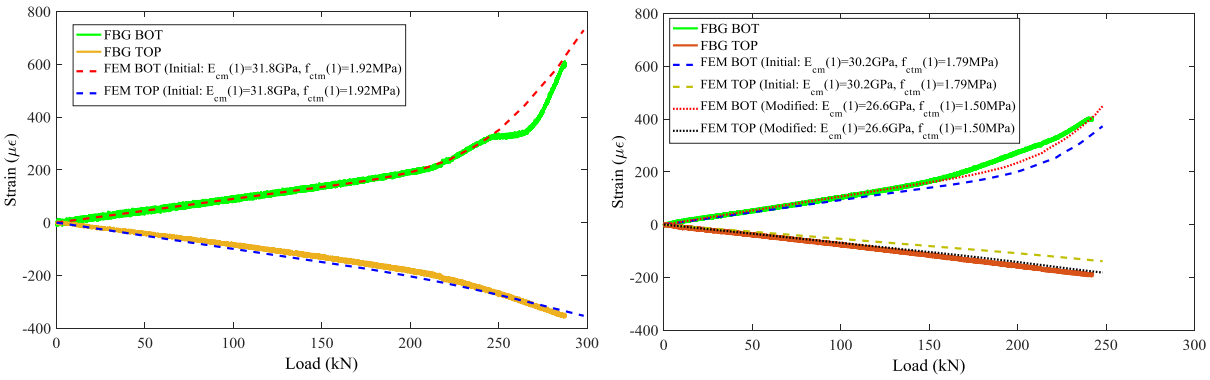

(a) Sleeper 312/8 **(b) Sleeper 360/7**

Figure 12. Comparison of FE analysis results and measured FBG sensor strains of sleepers during the bending test.

4.3 FE simulation of time-dependent effects

The final step of FE model development included incorporating additional time-dependent parameters (creep and shrinkage) to simulate the strain changes that occurred during the four month pre-service period. The built-in creep and shrinkage models provided in DIANA are based on Eurocode 2 EN 1992-1-1 (also refer to Table 3) [18]. The concrete creep coefficient

and the shrinkage strain development curves were first established for a given value of relative humidity according to the code-calculated relationships. These relationships were then used to estimate the total strain loss in the sleepers during the four month storage period. In developing these curves, an initial relative humidity of 70% was assumed (similar to the prestress loss calculations) which resulted in the calculation of an initial creep coefficient, $\varphi(t,t_0)$, of 1.06. An initial comparison between the measured and calculated strains (see Figure 13) revealed that the FE model overestimated the strain change during the storage period which indicated that either the creep strain, shrinkage strain or both were overestimated using the Eurocode equations. Therefore, a parametric study was undertaken in which the average ambient relative humidity was varied to calculate new values of shrinkage and creep strains which produced an overall strain response which better fit the FBG sensor measurements. A summary of the parametric study is presented in Figure 13 with strain change values reported at the centroid of the prestressing strands.

Material Model	RH	Creep and shrinkage parameters					
		$\varphi(t,t_0)$	$\Delta\varepsilon_{sh}(t)$ [με]	$\Delta\varepsilon_{cc}(t)$ [με]	$\Delta\varepsilon_{tot}$ [με]	$\varepsilon_{cc}(t)/\varepsilon_{tot}$	$\varepsilon_{sh}(t)/\varepsilon_{tot}$
MAT1	70%	1.06	274	254	528	0.48	0.52
MAT2	80%	0.90	238	214	452	0.47	0.53
MAT3	100%	0.51	127	122	249	0.49	0.51

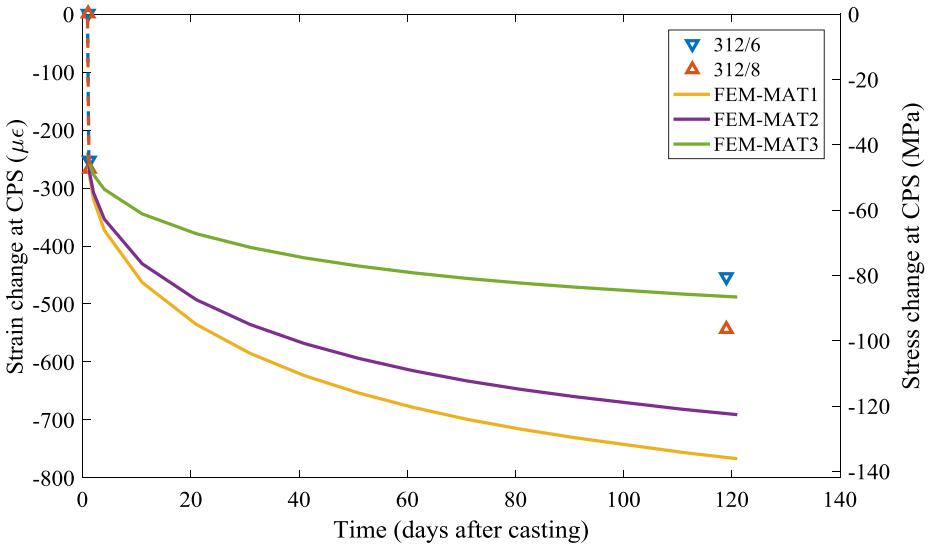

Figure 13. Comparison between fibre optic monitoring data and FE analysis of early-age strain change results (note baseline strain is taken at pre-detensioning)

The material model MAT3 provided the best fit to the FBG strain data. According to the FE analysis, 49% and 51% of the predicted strain change were estimated to be due to creep and shrinkage, respectively. The resulting values of strain were based on a creep coefficient, $\varphi(t_0,t)$, of 0.51 (48% of the initially predicted value) and a total shrinkage strain, $\varepsilon_{sh}(t)$, of 127 με (46% of the initially predicted value) for Group 312 sleepers at 119 days (4 months) after concrete casting. A relative humidity value of 100% was associated with the material model MAT3 however; this does not indicate that the actual average ambient relative humidity was 100% over the four month storage period. Instead, these results show that the Eurocode equations relating the relative humidity to the creep coefficient and shrinkage strains did not provide an accurate representation of the curing conditions experienced by the Group 312 sleepers.

5.0 Conclusions

Robust fibre optic strain sensor arrays were successfully developed and installed into twelve mass-produced prestressed concrete sleepers at a sleeper production facility. The sensor system was used to monitor the effect of production and early-age storage on the performance of the sleepers but was designed to last as long as the service life of the sleeper. Sensor measurement results were verified using Eurocode equations for predicting prestress loss and nonlinear finite element analysis. The main conclusions resulting from this work are as follows:

1. The feasibility of integrating robust FBG-based sensors within the manufacturing process of prestressed concrete sleepers was assessed during two separate installations. It was demonstrated that the system was capable of capturing strains while compensating for changes in temperature in four individual sleepers simultaneously during manufacturing and storage.

2. The integrated FBG sensors were able to provide a measurement of relative levels of performance variability due to the manufacturing process. Variation in strain among the various sleepers was found to be highest (COV = 0.14) for the curing period, and lowest (COV = 0.07) during detensioning. Sleeper Group 360 experienced 16% larger strain changes during the production process as compared with Group 312 sleepers. These sensor results highlight the inherent variability in strain development among identical sleepers and sleeper groups despite the relatively high levels of production quality control.
3. The sensor strain readings provided additional insights into the response of the sleepers during the bending qualification test. Strain readings revealed the assumed linear response region of the test became increasingly non-linear as the test proceed despite no visible cracks being observed. Therefore, although sleepers passed the qualification test, a refinement of what constitutes 'first cracking' should be based not on the first observable crack but on the first observed signs of non-linear load-strain response.
4. Eurocode-predicted instantaneous prestress losses underestimated the FBG-measured losses. However, the measured losses were found to be between only 45% and 49% of the total predicted losses during the first four months after casting. The sensing system was able to demonstrate that pre-service sleeper performance was well within the design limits.
5. A non-linear 3D finite element model of a typical prestressed concrete sleeper was developed and calibrated against the recorded fibre optic sensor strain results. A parametric study was conducted to assess the concrete creep and shrinkage characteristics independently. It was estimated that 49% of the total prestress loss during the storage period was due to creep and the remaining 51% was due to shrinkage. Using the sensor-validated finite element model, a creep coefficient of 0.51 was estimated for the first four

months following sleeper production which equated to 48% of the Eurocode-predicted value.

Acknowledgements

The authors gratefully acknowledge the EPSRC and Innovate UK for funding this research through the Cambridge Centre for Smart Infrastructure and Construction (CSIC) Innovation and Knowledge Centre (EPSRC grant reference number EP/L010917/1); the invaluable facilitation of the installation work from Andrew Carey, Paul Crowther and Stewart Smith of CEMEX; the on-site assistance of Jason Shardelow of the University of Cambridge and Jules Birks of Mott Macdonald (formerly University of Cambridge); and the technical assistance with sensor development from Cedric Kechavarzi and Philip Keenan of the University of Cambridge. Additional data related to this publication is available at the University of Cambridge data repository.

References

[1] Office of Rail and Road (ORR). Passenger rail usage 2015–16 statistical release. 2016:26pages.

[2] Network Rail. A better railway for a better Britain. 2013:40 pages.

[3] Carlsson S. Process induced prestress losses in long bed systems for railway sleepers. MSc Thesis. Chalmers University of Technology, Sweden, 2012: 300 pages.

[4] Taylor HPJ. The railway sleeper: 50 years of pretensioned, prestressed concrete. The Structural Engineer 1993; 71(16):281 – 295.

[5] Loaec A, Petit C, Lanticq V, Lamour V. Smart sleeper – measurement of bending moments in concrete sleepers laid on ballast tracks. Transport Research Arena, Paris La Defense, 2014: 6 pgs.

[6] Sadeghi J. Field investigation on dynamics of railway track pre-stressed concrete sleepers. Adv in Struct Engg 2010; 13(1):139 – 151.

[7] Kaewunruen S and Remennikov AM. Progressive failure of prestressed concrete sleepers under multiple high-intensity impact loads. Eng Struct 2009; 3:2460 – 2473.

[8] Lam HF, Wong MT, and Yang YB. A feasibility study on railway ballast damage detection utilizing measured vibration of in situ concrete sleeper. Eng Struct 2012; 45:284 – 298.

[9] Omondi B, Agellis DG, Sol H, Sitters C. Acoustic emission behaviour of prestressed concrete sleepers under quasi-static homologation testing. 31st Conference of the European Working Group on Acoustic Emission (EWGAE), 3 – 5 December, 2014:9 pgs.

[10] Chen Z, Shin M, Wei S, Andrawes B, Kuchma D. Finite element modeling and validation of the fastening systems and concrete sleepers used in North America. Proc IMechE Part F: J Rail and Rapid Transit; 228(6):590 – 602.

[11] Kaewunruen S and Remennikov A. Nonlinear finite element modelling of railway prestressed concrete sleeper. The 10th East Asia-Pacific Conference on Structural Engineering and Construction, August 3 – 5, 2006: 323 – 328.

[12] González-Nicieza C, Álvarez-Fernández MI, Menéndez-Díaz A., Álvarez-Vigil AE and Ariznavarreta-Fernández F. 2008. Failure analysis of concrete sleepers in heavy haul railway tracks. Eng Fail Anlys;15(1):90-117.

[13] McKeeman I, Fusiek G, Perry M, Johnston M, Saafi M, Niewczas P, Walsh M, and Khan S. (2016). First-time demonstration of measuring concrete prestress levels with metal-packaged fibre optic sensors. Smart Mater. Struct. 25:10 pages.

[14] Network Rail. Business Plan 2004 - Technical Plan, Section 9: Plans by Asset Type. 2004:66 pgs.

[15] Butler LJ, Gibbons N, Ping P, Xu J, Crowther P, MZEB Elshafie MZEB. Development of self-sensing concrete sleepers for next-generation rail infrastructure. Proceedings of the international conference on smart infrastructure and construction. Cambridge 27 – 29 June 2016. Institution of Civil Engineering Publishing:15 – 20.

[16] Ge Y, Elshafie MZEB, Dirar S, and Middleton CR. The response of embedded strain sensors in concrete beams subjected to thermal loading. Constr. Build. Mater. 2014; 70: 279 – 290.

[17] Kreuzer M. Strain measurement with fiber Bragg grating sensors. Technical Report HBM. Darmstadt Germany 2011:11 pages.

[18] EN 1992-1-1:2004 – Eurocode 2: Design of concrete structures – Part 1–1: General rules and rules for buildings. 2004.

[19] BS EN 13230-2-2009 Railway applications-track-concrete sleepers and bearers. British Standards Institution, 2009, Chiswick.

[20] Hendy CR, Smith DA. Designer's Guide to EN 1992-2 Eurocode 2: Design of Concrete Structures. Part 2: Concrete bridges. Thomas Telford Ltd. 2015:378 pages.

[21] Neville AM. Properties of Concrete, 5th Ed. Prentice Hall. 2005:846 pages.

[22] Bamforth P, Chisholm D, Gibbs J, and Harrison T. Properties of concrete for use in Eurocode 2. The Concrete Centre, 2008:59 pages. ISBN: 978-1-904482-39-0.

[23] Van Breugel K, Sule MS. Development of bond between reinforcement steel and early-age concrete. Finite Elements in Civil Engineering Applications: Proceedings of the 3rd DIANA World Conference, Tokyo, Japan, Eds MAN Hendriks and JG Rots 2002:149 – 156.

[24] TNO DIANA. DIANA v.10 User's manual, 2015.